Table Captions

Table S1. Descriptions of the sensitivity test simulations

Table S2. The OA mass concentration contributions from crop residue burning and its DRE due to absorption for the sensitivity test simulations.

Table S1. Descriptions of the sensitivity test simulations.

Simulation	Emission inventory	BC-to-OC ratio	OA absorptivity	Mixing state
K1.3_BASE	Comprehensive	0.27	$k_{OA}^{*} \times 1.3$	Shell/Core
K1.3_NOOACB	All without the OA emission from crop residue burning	0.27	$k_{OA}^{*} \times 1.3$	Shell/Core
K1.5_BASE	Comprehensive	0.27	$k_{OA}^{*} \times 1.5$	Shell/Core
K1.5_NOOACB	All without the OA emission from crop residue burning	0.27	$k_{OA}^{*} \times 1.5$	Shell/Core
RATIO0.18_BASE	Comprehensive	0.18	Saleh et al. (2014)	Shell/Core
RATIO0.18_NOOACB	All without the OA emission from crop residue burning	0.18	Saleh et al. (2014)	Shell/Core
RATIO0.18_NOBRC	Comprehensive	0.18	None	Shell/Core
RATIO0.42_BASE	Comprehensive	0.42	Saleh et al. (2014)	Shell/Core
RATIO0.42_NOOACB	All without the OA emission from crop residue burning	0.42	Saleh et al. (2014)	Shell/Core
RATIO0.42_NOBRC	Comprehensive	0.42	None	Shell/Core
VM_BASE	Comprehensive	0.27	Saleh et al. (2014)	Volume mixing
VM_NOCB	All without crop residue burning	0.27	Saleh et al. (2014)	Volume mixing

k_{OA}^{*}: the imaginary part of OA's refractive index, see equations (1), (2) and (3) (Saleh et al. 2014).

Table S2. The OA mass concentration contributions from crop residue burning and its DRE due to absorption for the sensitivity test simulations.

Testing item	Value	OA mass concentration contributions from crop residue burning (%)	crop residue burning OA DRE due to absorption (W m^{-2})
OA absorptivity	$k_{OA}^{*} \times 1.3$	30.3 [a]	+1.05 [e]
	$k_{OA}^{*} \times 1.5$	30.3 [b]	+1.22 [f]
BC-to-OC ratio	0.18	30.4 [c]	+0.96 [g]
	0.42	30.0 [d]	+0.81 [h]

[a] The differences of OA mass concentrations at surface between K1.3_BASE and K1.3_NOOACB divided by the corresponding OA mass concentration at surface in K1.3_BASE simulation, respectively.

[b] The differences of OA mass concentrations at surface between K1.5_BASE and K1.5_NOOACB divided by the corresponding OA mass concentration at surface in K1.5_BASE simulation, respectively.

[c] The differences of OA mass concentrations at surface between RATIO0.18_BASE and RATIO0.18_NOOACB divided by the corresponding OA mass concentration at surface in RATIO0.18_BASE simulation, respectively.

[d] The differences of OA mass concentrations at surface between RATIO0.42_BASE and RATIO0.42_NOOACB divided by the corresponding OA mass concentration at surface in RATIO0.42_BASE simulation, respectively.

[e] By multiplying the shortwave flux change differences between K1.3_BASE and NOBRC with the corresponding OA mass concentration contribution from crop residue burning.

[f] By multiplying the shortwave flux change differences between K1.5_BASE and NOBRC with the corresponding OA mass concentration contribution from crop residue burning.

[g] By multiplying the shortwave flux change differences between RATIO0.18_BASE and NOBRC with the corresponding OA mass concentration contribution from crop residue burning.

[h] By multiplying the shortwave flux change differences between RATIO0.42_BASE and NOBRC with the corresponding OA mass concentration contribution from crop residue burning.

Figure Captions

Figure S1. Time series of the (a) temperature and (b) relative humidity at 2 m above ground surface (T2 and RH2, respectively) and the (c) wind speed at 10 m above ground (WS10) observations (black dot) versus the corresponding WRF-Chem simulations (blue line) at three typical sites (Mengcheng, Suxian, and Xuzhou) in Eastern China in June 2013.

Figure S2. Time series of the observed (dots) and simulated (line) (a) $PM_{2.5}$, (b) sulfate, (c) ammonium and (d) nitrate mass concentrations ($\mu g/m^3$) at the Suixi site.

Figure S3. Spatial distributions of (a) carbonaceous aerosols mass concentration ($\mu g/m^3$) and (b) its contribution from crop residue burning (%) in the three typical hours (6:00) during the summer harvest in June 2013.

Figure S4. Scatterplots of simulated hourly AOD and corresponding MODIS AOD at 23 sites in June 2013. Normalized mean bias (NMB) and the correlation coefficient (R) are given in the scatterplot.

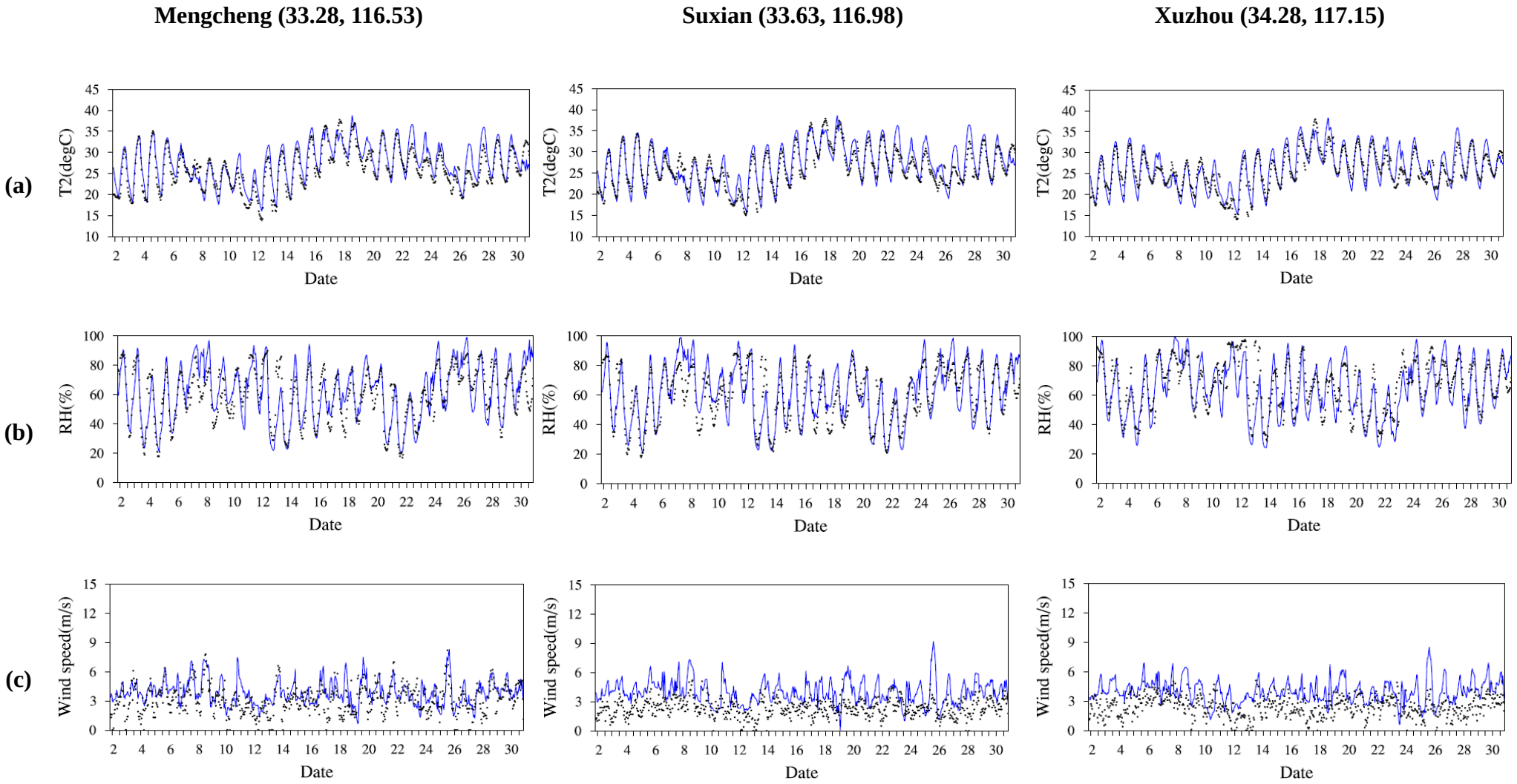

Figure S1. Time series of the (a) temperature and (b) relative humidity at 2 m above ground surface (T2 and RH2, respectively) and the (c) wind speed at 10 m above ground (WS10) observations (black dot) versus the corresponding WRF-Chem simulations (blue line) at three typical sites (Mengcheng, Suxian, and Xuzhou) in Eastern China in June 2013.

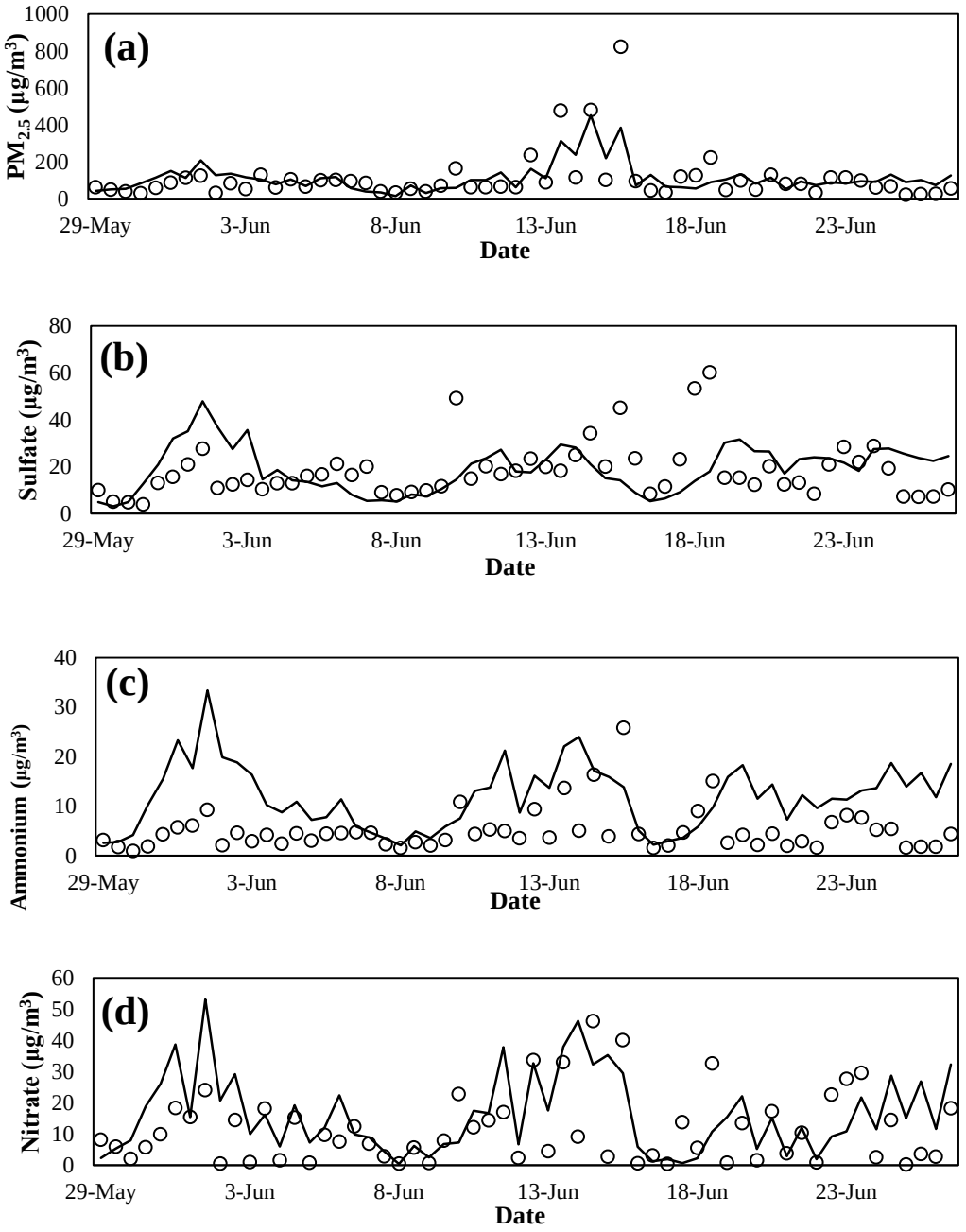

Figure S2. Time series of the observed (dots) and simulated (line) (a) $PM_{2.5}$, (b) sulfate, (c) ammonium and (d) nitrate mass concentrations ($\mu g/m^3$) at the Suixi site.

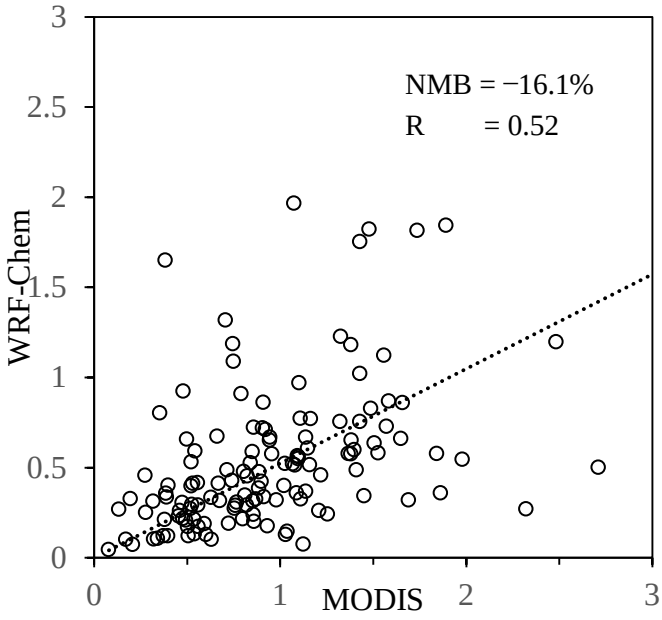

Figure S3. Scatterplots of simulated hourly AOD and corresponding MODIS AOD at 23 sites in June 2013. Normalized mean bias (NMB) and the correlation coefficient (R) are given in the scatterplot.